Melting of dust plasma crystals with defects

I. V. Schweigert,[1] V. A. Schweigert,[1] A. Melzer,[2] and A. Piel[2]
[1]*Institute of Theoretical and Applied Mechanics, Novosibirsk 630090, Russia*
[2]*Institut für Experimentelle und Angewandte Physik, Christian-Albrechts-Universität, 24098 Kiel, Germany*
(Received 7 December 1999)

The role of defects in the melting transition of a bilayer dust plasma crystal with vertical alignment is studied using Langevin molecular dynamics simulations. Two types of defects are considered: (i) point defects and dislocations and (ii) additional particles which are placed below and above the bilayer crystal (i.e., the so-called *strong* defects). It is shown that the presence of point defects and a few dislocations does not change the two-step melting scenario previously found for nondefect bilayer crystals. This contrast with the influence of the strong defects which leads to a substantial increase of the kinetic energy of particles and to local heating of the bilayer dust crystal.

PACS number(s): 52.25.Zb, 52.35.−g, 64.60.−i

I. INTRODUCTION

The melting transition in two-dimensional (2D) crystals of classical particles is one of the fundamental problems attracting experimental and theoretical studies for decades [1,2]. Experimental model systems for the study of 2D melting include electrons on the surface of liquid helium [3] and colloidal suspensions [4]. The plasma crystal is a rather new model system for the study of 2D crystalline structures [5–7]. Usually, plasma crystals consist of micrometer size dust particles trapped in the electrode sheath of gaseous discharges by the balance of gravitational and electric field forces. The dust particles attain a high negative charge Z of the order of 10^3–10^5 of elementary charges due to the inflow of plasma ions and electrons. In experimental systems [8–11] the dust crystals in the sheath are of large extent in the horizontal plane, but of only a few (1–20) crystal layers in the vertical direction. In the horizontal plane the particles form the usual hexagonal lattices, whereas vertically the negatively charged microparticles are arranged in aligned chains. This is not the most energetically favorite structure for the screened Coulomb isotropic potential of interactions. The vertically aligned particle arrangement indicates that a Debye-Hückel model of interparticle interactions breaks down in a plasma with streaming ions.

Moreover, experiments [5,6] have shown that a decrease of gas pressure causes a dramatic change of the state of the system which is associated with crystal heating and melting. This experimental finding is surprising because for 2D and 3D close-packed crystals with isotropic interparticle interactions the statistical properties of the system are not affected by a change of the viscosity of the surrounding medium. The viscosity sets only the time scale of particle motion unless hydrodynamic interactions should be taken into account [4]. Nevertheless, in the case of dust crystal in the sheath a decrease of pressure amplifies particle oscillations and the particle kinetic energy increases by orders of magnitude. Note that the temperature of the surrounding gas and the charge of particles remain unchanged.

The phenomenon of particle alignment in ion flux was considered within a collisionless approach in [12], using a fluid approximation in [13], and in the collision case in [14,15]. It was found that the ion flux is focused by negatively charged particles, which leads to the formation of areas of enhanced ion density behind the upstream particles. These areas provide an attractive force for lower particles and explain the vertical alignment of particles. From more advanced theoretical studies [14–16] and experiments [17,18] it has been shown that the attraction due to the ion clouds is asymmetric. Each ion cloud provides an attractive force for all other particles of the crystal, but there is no interaction with its parent upstream particle. The asymmetry of particle screening and the nonpotential character of interparticle interactions leads to the development of an instability.

The mechanism of dust particle heating was explained in Refs. [14,15]. Linear analysis of particle motion equations shows that an instability develops when the dust-neutral gas friction becomes less than some critical value ν_{in}. A detailed study of the melting of a nondefect bilayer crystal in the sheath was carried out using Langevin molecular dynamics (MD) simulations [7,19]. It was shown that the melting of the bilayer crystal is a two-step process. With decreasing of gas friction first the instability predicted from the linear analysis [14,15] sets in at ν_{in} and the crystal transits to a ''hot'' crystalline state with developed oscillations. A further decrease of the friction coefficient to the second critical value $\nu_\star$ causes the bilayer crystal to melt. From MD simulations the kinetic energy of particle motion as a function of gas friction was obtained which agrees with the experimental data within an order of magnitude.

However, one feature of the experimental observation still needs an explanation. In our simulations the particle kinetic energy quickly increases at the critical friction value, whereas in the experiment the particle energy increases more smoothly within a wide range of gas friction. The experimental system first shows the formation of heated spots and then both liquidlike areas and crystalline patches appear in the crystal. With further reduced friction, streamline particle motion takes over more and more, finally leading to a liquid state [5].

In our earlier studies we have treated the nondefect bilayer crystal and defects appearing only close to the melting temperature. In the experimental system the dust crystals

have point and extended defects in the lattices and additional particles which are placed above and below the main layers.

In this article, we study the melting of the bilayer crystal with both kinds of defects observed in the experiment. The first type of defects are vacancies, interstitials, and uncorrelated diclocations which are typical for 2D structure and destroy the translational and the angular order. The second type are the additional particles which surround the bilayer crystal above and beneath (so-called *strong defects*).

II. MODEL OF THE BILAYER CRYSTAL WITH DEFECTS

The melting of the defect bilayer crystal is studied using a previous model of dust crystal in the sheath [14,15]. In this model, the following are assumed: (i) The particles move in the plane parallel to the electrode. This simplification follows from experimental observations which show that dust particles move mainly in the horizontal (x,y) plane. The amplitude of particle oscillations in the vertical z direction is comparably small due to the strong vertical confinement formed by the gravitational and the electrical forces. (ii) The asymmetric ion distribution around the particle is replaced by a uniform ion distribution and an effective positive charge Z_c placed below the parent dust particle. The value and coordinates of effective positive charges are taken from Refs. [7,15]. (iii) Each ion cloud (i.e., positive point charge) is rigidly connected to the upper parent particle. This is justified since a shift of the upstream particle immediately leads to the redistribution of the ion density around this particle [14,15], because the characteristic time of ion motion is much less than the time scale of dust particle motion.

In our earlier works [7,14,15,19] we have considered bilayer crystals which are infinite in the horizontal plane. We took a fragment of the crystal with periodic boundary conditions. Here, we consider a finite bilayer cluster because in the crystalline phase the defects are easily formed due to the presence of the external boundary of the system.

The particles interact through the screened Coulomb potential $V(\vec{r}_i,\vec{r}_j)=(Z^2/|\vec{r}_i-\vec{r}_j|)\exp(-\kappa|\vec{r}_i-\vec{r}_j|)$, where $\vec{r}_i$ is the coordinate of the ith particle, and $1/\kappa$ is the screening length which is $\kappa=2/a$ [20,21], where a is the mean interparticle distance.

The bilayer crystal consists of 996 particles. In the crystal phase the particles are arranged into two parallel almost hexagonal lattices in the (x,y) plane with a vertical distance d. In the vertical direction the particles and the charges are aligned as observed in the experiment. The two layers contain the same number of particles.

The Langevin equations of particle motion in such a crystal can be written as [7]

$$\frac{d^2\vec{r}_i}{dt^2}=\frac{1}{M}\vec{F}_i-\nu\frac{d\vec{r}_i}{dt}+\frac{1}{M}\vec{F}_l-\frac{1}{M}\vec{\nabla}U(\vec{r}_i), \tag{1}$$

where M is the mass of a dust particle, $\vec{F}_i$ is the electrostatic interaction force between the dust particles and ion clouds, ν is the friction coefficient of the dust particles with the neutral gas, and $\vec{F}_l$ is the Langevin force corresponding to the room temperature of the surrounding neutral gas. U is an external potential which confines the system to the radial plane.

The electrostatic interaction force acting on the dust particles can be written as [15]

$$\vec{F}_i=Z^2\sum_j\frac{\vec{r}_i-\vec{r}_j}{|\vec{r}_i-\vec{r}_j|^3}e^{-\kappa|\vec{r}_i-\vec{r}_j|}(1+\kappa|\vec{r}_i-\vec{r}_j|)$$
$$-ZZ_c\sum_n\frac{\vec{r}_i-\vec{r}_n}{|\vec{r}_i-\vec{r}_n|^3}e^{-\kappa|\vec{r}_i-\vec{r}_n|}(1+\kappa|\vec{r}_i-\vec{r}_n|), \tag{2}$$

where j, n denote the summation over all layers of particles and charges, respectively. The first term in Eq. (2) describes the interparticle repulsion and the second term refers to the attraction between a particle and positive charges. Note that a particle does not interact with its downstream positive charge which mimics the asymmetric ion distribution around a particle. The coordinates of charges $\vec{r}_n=\vec{r}_j-d_c\vec{e}_z$, where d_c is the distance between a positive charge and the lower layer in the vertical direction.

The external potential is taken as

$$U(r_i\leqslant R^*)=0,\ U(r_i>R^*)=\alpha(r_i-R^*)^2, \tag{3}$$

where $R^*=0.45$ cm and $\alpha=10^5$ eV/cm^2. The external confinement was chosen in such a way that the particle density in the simulations coincides with the experimental one. Other simulation parameters are taken from experiment [5]. The dust particle radius is $R=4.7$ μm, corresponding to a dust mass $M=6.73\times10^{-13}$ kg. The dust charge is $Z=16\,000$ of elementary charges, the interparticle distances $a=450$ μm, and the interlayer distances $d=0.8a$. In the simulations the positive charge is taken to be $Z_c=0.5Z$ with a vertical distance $d_c=0.6a$ [15]. The corresponding dust plasma frequency for the experimental conditions then is $\omega_{\rm pd}=\sqrt{Z^2e^2/\epsilon_0Ma^3}=110$ s^{-1}. The transition from solid crystal structure to the gaslike state in the experiment is observed by reducing the pressure from 120 Pa down to 40 Pa corresponding to an Epstein dust-neutral friction coefficient $\nu=32$ s^{-1} down to 10 s^{-1} [22]. Below the dimensionless friction constant ν/ω_{pd} is used.

III. MELTING OF THE BILAYER CRYSTAL WITH POINT DEFECTS AND DISLOCATIONS

The first type of defects such as vacancies, interstitials, and dislocations in the crystal are created by cooling the system from the high-temperature liquid state. Initially, at high temperature the particles are placed randomly within the area $r<R^*$. Then with a slow numerical decreasing of temperature the particles form a hexagonal lattice with a certain amount of point and extended defects. Note that an infinite crystal with defects relaxes to a perfect hexagonal lattice during slow numerical freezing.

In order to investigate the influence of defects on the melting process the crystal shown in Fig. 1 is taken, which is a typical example of the bilayer crystal with the first type of defects. It contains uncorrelated dislocations with Burgers vectors equal to 2. Additionally, the crystal has a lot of defects near the external boundary, since the hexagonal structure can be fitted into a circle only with a number of point defects. The lower layer has the same structure. In the simulations at each value of the friction 2×10^4–6×10^4 MD

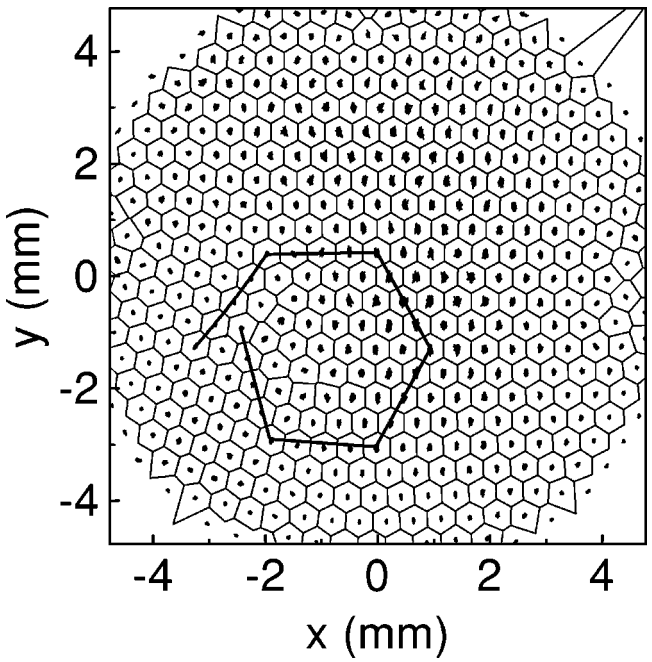

FIG. 1. Particle trajectories in the upper layer of the dust crystal with point defects and dislocations at $\nu=0.0721\omega_{\mathrm{pd}}$. The Burgers vector of uncorrelated dislocations is equal to 2.

steps are executed first in order to reach the steady-state behavior and then the characteristic parameters are obtained by averaging over time. We assume that the steady state is reached when the averaged kinetic energy of the particles remains constant during a run.

The dynamics of particle motion is studied by reducing the friction coefficient which corresponds to decreasing the gas pressure in the discharge. The mean kinetic energy of particles in the upper layer E as a function of friction coefficient ν/ω_{pd} is shown in Fig. 2(a) (solid circles). At high gas friction the system has crystalline structure and the energy E is about the temperature of the surrounding gas. Decreasing the friction to the critical value ν_{in} only slightly changes the system in spite of the presence of defects [Fig. 2(a), regime I]. In the vicinity of the critical friction value $\nu_{in}=0.105\omega_{pd}$ the energy E quickly rises from 0.1 to 2 eV and the system transits to the ''hot'' crystalline regime which is characterized by developed particle oscillations [Fig. 2(a), regime II]. Note that this first critical value is close to the critical friction of an instability for the nondefect bilayer crystal derived from a linear analysis [14,15]. In the next range of gas friction, $\nu_{*}<\nu<\nu_{in}$, the bilayer crystal passes through a sequence of ''hot'' crystalline states and the kinetic energy of particles rises from 2 to 7 eV. In fact, Fig. 1 shows the particle trajectories just before melting which were taken at $\nu=0.0721\omega_{\mathrm{pd}}$ (regime II, $E=7$ eV). It is clearly seen that the particle trajectories do not display signs of dislocations. The bilayer crystal retains crystalline order in regime II, even though the coupling parameter which is the interparticle interaction energy, measured in units of the particle kinetic energy $\Gamma=Z^2e^2/aE$, falls from 150 to 52 in this range of friction. The bilayer crystal with point and extended defects exhibits an enhanced stability against thermal fluctuations as well as nondefect bilayer crystal [7]. Note that a single-layer crystal with the symmetric screened ($\kappa=2/a$)

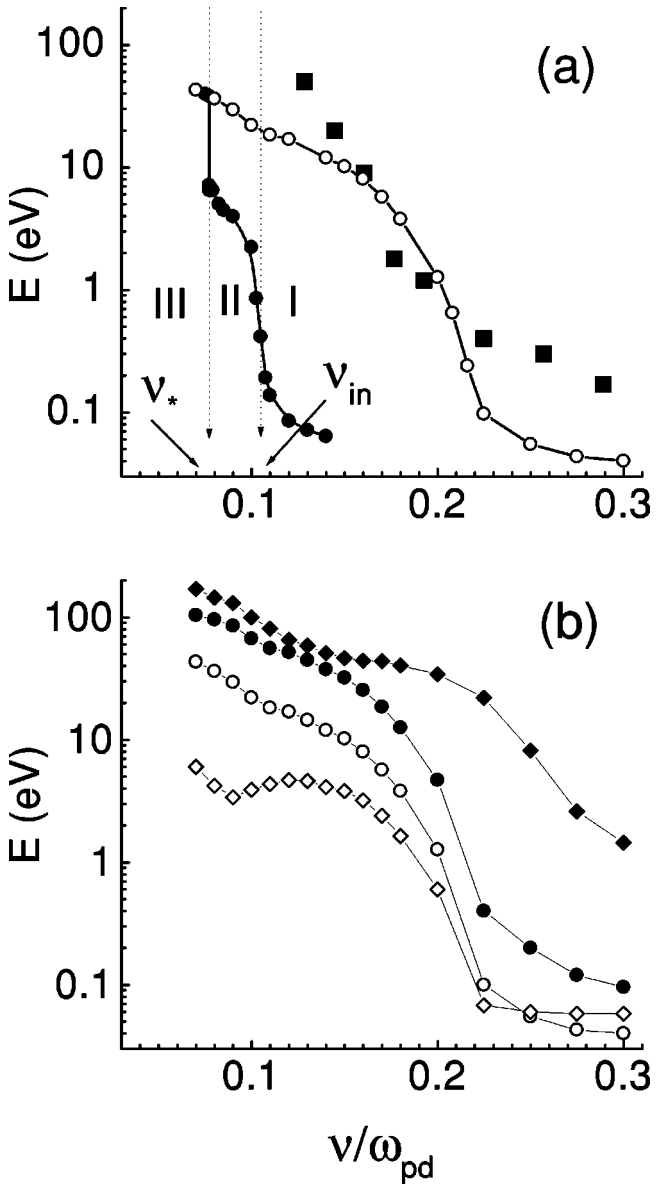

FIG. 2. (a) Mean kinetic energy of the dust particles as a function of the gas friction coefficient for the bilayer crystal with point defects and dislocations (solid circles) and with strong defects (open circles). The experimental values [5] are also shown for comparison (solid squares). (b) Mean kinetic energy of the dust crystal with strong defects for the top incomplete layer (open diamonds), the upper lattice (open circles), the lower lattice (solid circles), and the bottom incomplete layer (solid diamonds) as a function of the gas friction constant.

potential of interaction melts at $\Gamma_{*}=189$ [7].

With further friction decreasing at the second critical value $\nu_{*}=0.0720\omega_{pd}$ the formation of temperature-induced defects is observed and the system transits to the isotropic liquid [Fig. 2(a), regime III]. The phase transition is accompanied by a jump of the kinetic energy of particles.

To identify the critical points in more detail we calculate the diffusion coefficient which can be written as

$$D=\sum_{i=1}^{N}\left\{\Delta\vec{r}_i(t)^2-\left[\sum_{j=1}^{N}\Delta\vec{r}_j(t)\right]^2/N\right\}/N4t, \qquad (4)$$

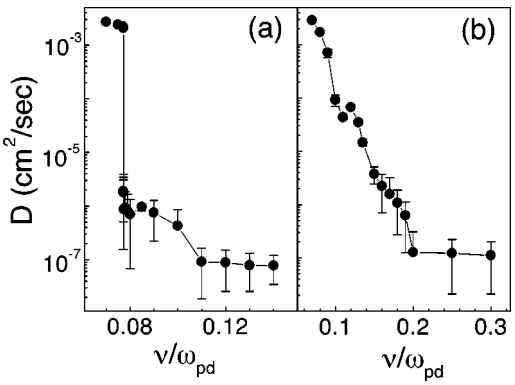

FIG. 3. Diffusion coefficient as a function of the gas friction coefficient for the bilayer crystal with point defects and dislocations (a) and with strong defects (b).

where $\Delta\vec{r}_i(t)=\vec{r}_i(t)-\vec{r}_i(0)$. In Fig. 3 the diffusion coefficient is shown as a function of friction coefficient. In the crystalline state (regimes I and II) the diffusion is small and it jumps at the melting point ν_* by 3 orders of magnitude [see Fig. 3(a)].

Furthermore, the mode spectra are analyzed, which allows one to clarify features of particle motion in the different regimes. These spectra are derived from the particle velocity autocorrelation function by a Fourier transform. The excitation spectra Z_ω can be written as

$$Z_\omega(\omega)=2\int_0^\infty e^{i\omega\tau}Z_v(\tau)d\tau,$$

$$Z_v(\tau)=\sum_j \frac{\langle\vec{v}_j(t)\vec{v}_j(t-\tau)\rangle}{\langle\vec{v}_j(t)\vec{v}_j(t)\rangle}, \qquad (5)$$

where $\vec{v}_j$ is the velocity of the jth particle and $\langle\cdot\rangle$ denotes the average over time. The spectra of particle oscillations are given in Fig. 4. At high pressure in the crystalline state ($\nu=0.14\omega_{pd}$, regime I) the crystal has a quite broad spectrum which is typical for 2D Coulomb systems [see Fig. 4(a)]. The

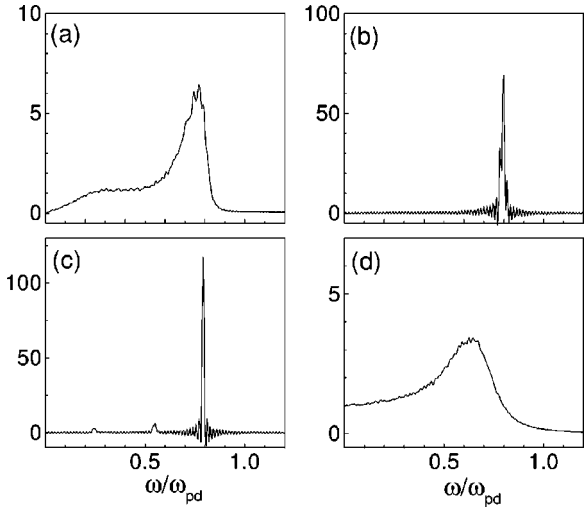

FIG. 4. Phonon spectra of the bilayer crystal with point defects and dislocations at different friction coefficients $\nu=0.14\omega_{pd}$ (a), $\nu=0.105\omega_{pd}$ (b), $\nu=0.0721\omega_{pd}$ (c), and $\nu=0.0720\omega_{pd}$ (d).

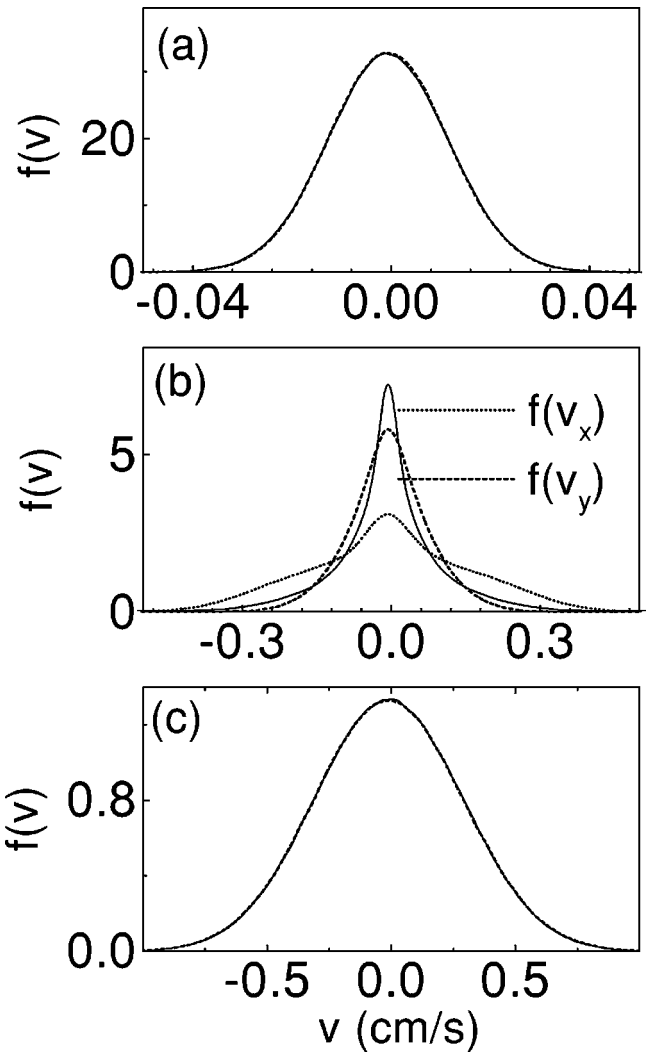

FIG. 5. Particle velocity distribution function at different friction coefficients $\nu=0.14\omega_{pd}$ (a), $\nu=0.0721\omega_{pd}$ (b), and $\nu=0.0720\omega_{pd}$ (c). (The dashed and dotted lines denote results of the MD simulations; solid lines are the Maxwellian PVDF for comparison.)

particle velocity distribution function (PVDF) in this regime is a Maxwellian one [see Fig. 5(a)]. At $\nu=0.105\omega_{pd}$ and $\nu=0.0721\omega_{pd}$ (regime II, ''hot'' crystalline states) the spectra have a sharp peak denoting the appearance of unstable particle oscillations [see Figs. 4(b) and 4(c)]. These peaks are found at quite high frequency close to the dust plasma frequency. It should be emphasized that the crystal structure is destroyed by long-wave (low-frequency) phonons; thereby the observed short-wave (high-frequency) oscillations are not dangerous to the crystal structure. In the ''hot'' crystalline state the PVDF differs from the Maxwellian [Fig. 5(b)]. At the second critical value of the friction, ν_*, the bilayer crystal undergoes a melting transition. The spectrum becomes broad and includes zero-frequency modes [Fig. 4(d)] which lead to the destruction of the crystal structure. As expected in the liquid state the PVDF again is an isotropic Maxwellian [Fig. 5(c)].

Note that this ''hot'' crystalline regime does not appear during the melting of bilayer crystals with an isotropic Coulomb or screened potential of interactions [23]. The origin of

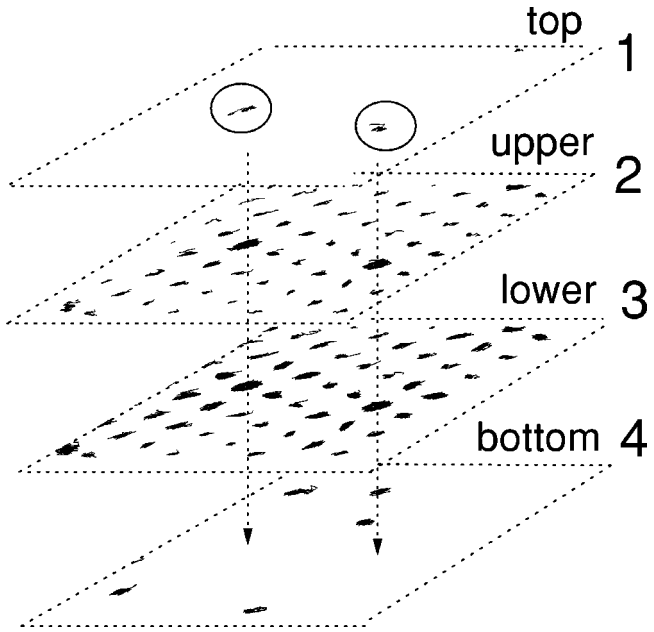

FIG. 6. Scheme of the bilayer crystal with strong defects: the top incomplete layer (1), the upper lattice layer (2), the lower lattice layer (3), and bottom incomplete layer (4).

the two-step melting mechanism of the aligned bilayer crystal is the instability of the system against short-wave oscillations. On the basis of these results we can conclude that the occurrence of points defects and dislocations only slightly increases the particle temperature. As a whole the melting process of a bilayer crystal with the first type of defects turns out to be similar to the melting behavior of the nondefect bilayer crystal [7,19].

IV. MELTING OF A BILAYER CRYSTAL WITH STRONG DEFECTS

Here, the influence of additional particles above and below a bilayer crystal on the melting transition is studied. A four-layer structure is analyzed which consists of the top incomplete layer, two hexagonal lattices with point defects and dislocations, and the bottom incomplete layer (see Fig. 6). The number of particles in the top and bottom incomplete layers is 45, corresponding to 5% of the total number of particles. The particles interact through a short-range screened potential; therefore this number of particles is too small to form a lattice. Initially, the particles in the top and bottom layers are placed randomly. The system is equilibrated during 10^4–5×10^4 MD steps, and top and bottom particles occupy the aligned sites. The vertical distance between incomplete layers and the main lattices is the interlayer distance d.

We study the behavior of the bilayer crystal, gradually lowering the gas friction. Solving Eq. (1), we calculate the electrostatic interaction force acting on a particle, performing a summation over all particles of four layers and all positive

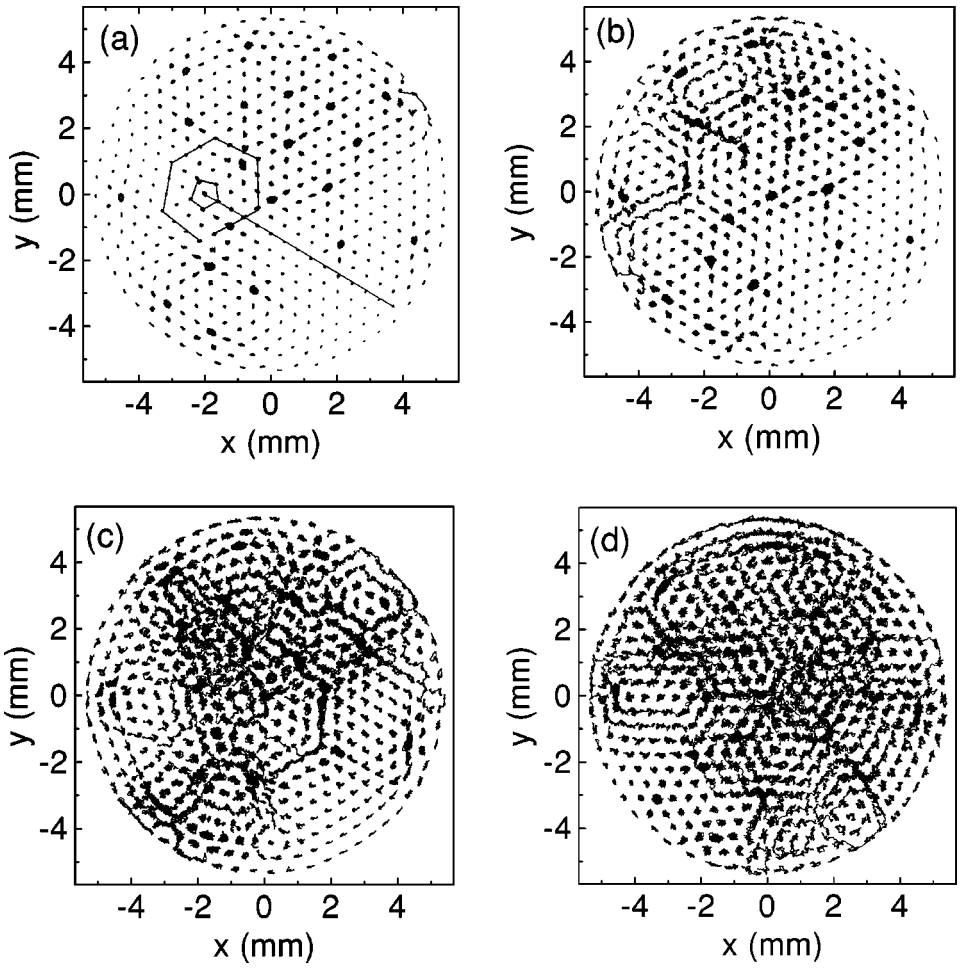

FIG. 7. Particle trajectories in the upper layer of the bilayer crystal with strong defects at $\nu=0.15\omega_{pd}$, $E=10$ eV (a), at $\nu=0.14\omega_{pd}$, $E=12$ eV (b), at $\nu=0.13\omega_{pd}$, $E=14.5$ eV(c), and at $\nu=0.12\omega_{pd}$, $E=17$ eV (d). The dislocation with Burgers vector of length 1 and the ''pentagon'' are marked by lines (a).

charges of four layers except a positive charge under this particle.

At high gas friction the system with strong defects also exhibits a crystalline structure. However, the presence of top and bottom particles leads to an increase of the kinetic energy of particles compared to the case of the first type of defects [see Fig. 2(a) (open circles)]. The calculated kinetic energy is now in quite close quantitative agreement with the experimental values (solid squares). Figure 2(b) shows the kinetic energy of particles in the upper (open circles) and lower (solid circles) crystal layers and in the incomplete top layer (open diamonds) and bottom one (solid diamonds). The particles in each layer have different temperatures and the amplitude of particle oscillations increases when going from the top to the bottom layer. It is noteworthy that even for high gas friction the kinetic energy of the bottom particles is much higher than that of the other layers. Note that the particle densities in the top and bottom incomplete layers are about the same. Despite the high kinetic energy, the bottom particles weakly heat the nearest lattice [see Fig. 2(b)].

With decreasing the gas friction instability sets in which in the presence of strong defects is at $\nu=0.216\omega_{pd}$. In Fig. 7 the particle trajectories in the upper layer are plotted for different ''hot'' crystalline regimes. At friction constant $\nu=0.15\omega_{pd}$ the upper layer has an ordered structure and an uncorrelated dislocation with a Burgers vector equal to 1 is clearly seen [see Fig. 7(a)]. The particles oscillate with large amplitude, but the motion of some of the particles is more violent. We found that these particles are placed exactly under the particles of the top incomplete layer (see Fig. 6). At lower friction $\nu=0.14\omega_{pd}$ streamline motion is formed around the ''pentagon'' related to the uncorrelated dislocation, Fig. 7(b). At $\nu=0.13\omega_{pd}$ and $\nu=0.12\omega_{pd}$ the lattice melts locally and liquid fragments form first under the top particles, Figs. 7(c) and 7(d). The particles of the lower crystal layer, in general, show the same motion than those in the upper crystal layer, but their oscillations are more prominent. To illustrate the role of top and bottom particles in the heating enlarged fragments of both crystal layers at $\nu=0.135\omega_{pd}$ are given in Fig. 8. It is apparent that the layers are mostly influenced by particles from the top incomplete layer. The most effectively heated particles in the fragments (marked by 1 in Fig. 8) are in a vertical chain with a top particle. In both layers these particles rotate around their equilibrium positions. At this value of the gas friction the kinetic energy of bottom particles is very high (about 60 eV). The positions of particles in the bottom incomplete layer are denoted by 2 and 3. Their influence on the neighboring layer is very small [see Fig. 8(b)].

The reason for the dominant role of particles of the top incomplete layer is the attraction of the lower particles and the positive charge created by the top particle, which forces the particle beneath to follow the motion of the top particle. The particles in the bottom incomplete layer affect the nearest layer only through Coulomb repulsion. Nevertheless, with increasing kinetic energy of these bottom particles their influence on the lower layer becomes larger.

It should be underlined here that in the case of strong defects the onset of instability provides a considerable increase of the mean kinetic energy, but it increases more smoothly than in the case of the bilayer crystal with point

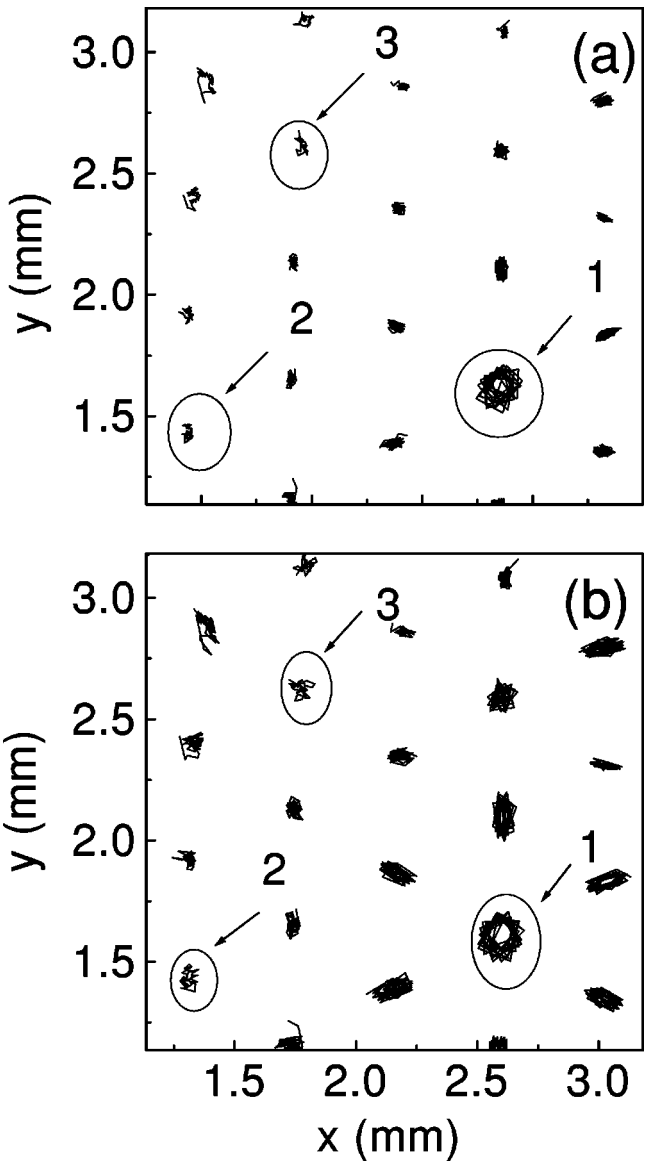

FIG. 8. Particle trajectories in a fragment of the upper (a) and lower layer (b) with one particle in the top incomplete layer and two particles in the bottom one at $\nu=0.135\omega_{pd}$. (1 denotes the position of the top particle and 2,3 refer to the bottom particle positions.)

defects and dislocations. The diffusion coefficient given in Fig. 3(b) also shows features of a continuous melting. The two-step melting transition is smeared out by local heating effects and it is difficult to identify a point of melting.

To gain additional insight into the role of the particles in the bottom incomplete layer for crystal heating, the melting of the bilayer crystal is studied with only a few bottom particles and no particles in the top incomplete layer. This structure consists of two hexagonal crystal layers and a bottom incomplete layer with three particles. The trajectories of the lower lattice and bottom particles at $\nu=0.12\omega_{pd}$ are plotted in Fig. 9. In this case it is found that the particle temperature change is similar to the case of the bilayer crystal *without* strong defects. The three bottom particles have a large kinetic energy which coincides with the energy of the bottom layer considered above. The directed velocity of bottom particles is quite large and one particle has an almost linear trajectory. This high-energy particle moving beneath is scat-

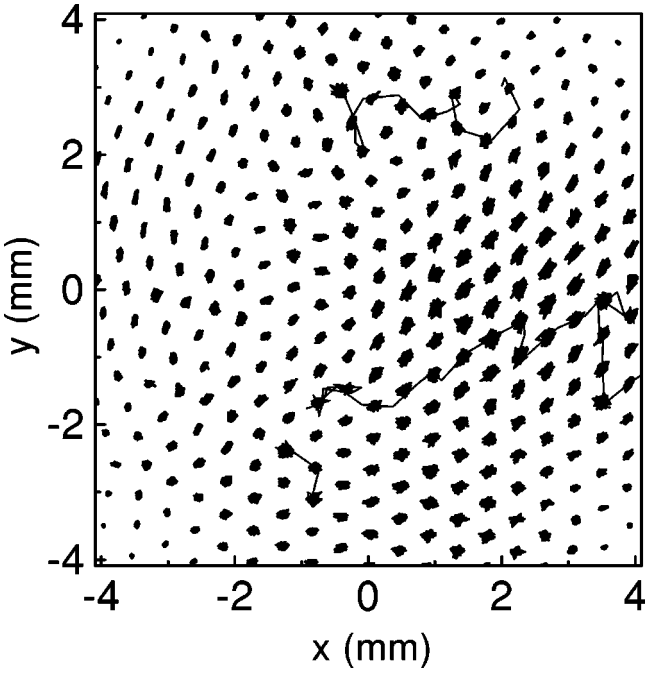

FIG. 9. Particle trajectories in the lower lattice of the bilayer crystal with only three bottom particles at $\nu=0.12\omega_{pd}$. The extended trajectories refer to three bottom particles.

tered by the nearest lattice particles due to Coulomb repulsion and transfers the momentum of motion to the lattice. In Fig. 9 it is clearly seen that the part of the lattice above the extended particle trajectory is heated. It is interesting to note that the bottom particles move through the potential minima which are situated under the particles of the nearest lattice. One might speculate that this mechanism leads to the lower layer fast moving particles used in a recent experiment to generate Mach cones in plasma crystals [24].

V. CONCLUSION

In conclusion, we have performed Langevin molecular dynamics simulations to reveal the role of two types of defects in melting of the aligned bilayer crystal. It was found that the bilayer crystal with point defects and uncorrelated dislocations exhibits a two-step melting dynamics close to the nondefect bilayer crystal described earlier [7,19]. The instability is induced by decreasing gas friction and leads to the quick rise of the kinetic energy of particle motion. The system transits to the ''hot'' crystalline regime with strong oscillations. With further decreasing of the gas friction the system undergoes a melting transition.

It was shown that the bilayer crystal with strong defects has a more complex mechanism of particle heating. In this case the melting is governed by global heating by self-excited oscillations and the local heating by strong defects as well. The top particles play the most important role in the heating since in the aligned structure the top particle determines the motion of particles in the vertical chain. The bottom particles affect the nearest lattice only by means of Coulomb repulsion; thereby only high-energy bottom particles can heat only the nearest layer.

ACKNOWLEDGMENTS

We would like to thank the Deutsche Forschungsgemeinschaft (436 RUS 113/183/1,2) and INTAS-RFBR (IR-97-775) for financial support.

[1] M.A. Glaser and N.A. Clark, in *Advances in Chemical Physics*, Vol. LXXXIII, edited by I. Prigogine and S. A. Rice (Wiley, New York, 1993), p. 543.
[2] K.J. Strandburg, Rev. Mod. Phys. **60**, 161 (1988).
[3] C.C. Grimes and G. Adams, Phys. Rev. Lett. **42**, 795 (1979).
[4] K. Zahn, J.M. Mendez-Alcaraz, and G. Maret, Phys. Rev. Lett. **79**, 175 (1997).
[5] A. Melzer, A. Homann, and A. Piel, Phys. Rev. E **53**, 2757 (1996).
[6] H. Thomas and G.E. Morfill, Nature (London) **379**, 806 (1996).
[7] V.A. Schweigert, I.V. Schweigert, A. Melzer, A. Homann, and A. Piel, Phys. Rev. Lett. **80**, 5345 (1998).
[8] J.H. Chu and L. I, Phys. Rev. Lett. **72**, 4009 (1994).
[9] H.M. Thomas, G.E. Morfill, G.V. Dumel, J. Goree, B. Feuerbacher, and D. Möhlmann, Phys. Rev. Lett. **73**, 652 (1994).
[10] Y. Hayashi and K. Tachibana, Jpn. J. Appl. Phys., Part 2 **33**, L804 (1994).
[11] A. Melzer, T. Trottenberg, and A. Piel, Phys. Lett. A **191**, 301 (1994).
[12] S.V. Vladimirov and M. Nambu, Phys. Rev. E **52**, 2172 (1995).
[13] F. Melandsø and J. Goree, Phys. Rev. E **52**, 5312 (1995).
[14] A. Melzer, V.A. Schweigert, I.V. Schweigert, A. Homann, and A. Piel, Phys. Rev. E **54**, 46 (1996).
[15] V.A. Schweigert, I.V. Schweigert, A. Melzer, A. Homann, and A. Piel, Phys. Rev. E **54**, 4155 (1996).
[16] V.A. Schweigert, V.M. Bedanov, I.V. Schweigert, A. Melzer, and A. Piel, JETP **88**, 482 (1999).
[17] A. Melzer, V.A. Schweigert, and A. Piel, Phys. Rev. Lett. **83**, 3194 (1999).
[18] K. Takahashi, T. Oishi, K. Shimomai, Y. Hayashi, and S. Nishino, Phys. Rev. E **58**, 7805 (1998).
[19] I.V. Schweigert, V.A. Schweigert, A. Melzer, and A. Piel, JETP **87**, 905 (1998).
[20] A. Homann, A. Melzer, S. Peters, R. Madani, and A. Piel, Phys. Rev. E **56**, 7138 (1997).
[21] A. Homann, A. Melzer, R. Madani, and A. Piel, Phys. Lett. A **242**, 173 (1998).
[22] P.S. Epstein, Phys. Rev. **23**, 710 (1924).
[23] I.V. Schweigert, V.A. Schweigert, and F.M. Peeters, Phys. Rev. Lett. **82**, 5293 (1999).
[24] D. Samsonov, J. Goree, Z.W. Ma, A. Bhattacharjee, H.M. Thomas, and G.E. Morfill, Phys. Rev. Lett. **83**, 3649 (1999).